Analytica Chimica Acta 1181 (2021) 338910

Contents lists available at ScienceDirect

Analytica Chimica Acta

journal homepage: www.elsevier.com/locate/aca

Development of a novel label-free all-fiber optofluidic biosensor based on Fresnel reflection and its applications

Wenjuan Xu [1], Yuxin Zhuo [1], Dan Song [1], Xiangzhi Han, Jiaxin Xu, Feng Long*

School of Environment and Natural Resources, Renmin University of China, Beijing, 100872, China

HIGHLIGHTS

- Simple, compact, cost-effective, and robust LF-AOB was built based on Fresnel reflection and all-fiber structure..
- LF-AOB can *in situ* real-time detect various solution concentrations in optofluidic systems with the high sensitivity.
- One-point calibration method based on proposed theory is conducive for rapid and convenient detection of targets.
- LF-AOB can detect spike protein receptor-binding domain (S-RBD) with the LOD of 0.005 ng/mL.
- LF-AOB can extend as label-free universal platform with easy-of-modification of biorecognition elements.

GRAPHICAL ABSTRACT

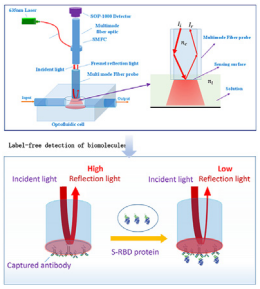

ARTICLE INFO

Article history:
Received 23 June 2021
Received in revised form
1 August 2021
Accepted 2 August 2021
Available online 4 August 2021

Keywords:
Refractive index sensor
All-fiber optical system
Fresnel reflection
Optofluidics
SARS-Cov-2

ABSTRACT

A novel, compact, cost-effective, and robust label-free all-fiber optofluidic biosensor (LF-AOB) based on Fresnel reflection mechanism was built through integrating single-multi mode fiber coupler and highly sensitive micro-photodetector. The Fresnel reflection light intensity detected by the LF-AOB greatly depended on the RI change on the end-surface of the fiber probe according to experimental and simulation results. The capability of the LF-AOB for real-time *in situ* detection in optofluidic system were verified by measuring salt and protein solution, and the lowest limit of detection was 1.0×10^{-6} RIU. Our proposed theory can effectively eliminate the influence of light intensity fluctuation, and one-point calibration method of sensor performance is conducive for rapid and convenient detection of targets. Label-free sensitive detection of SARS-Cov-2 Spike protein receptor-binding domain (S-RBD) and the binding kinetics assay between S-RBD and anti-S-RBD antibody were achieved using the LF-AOB. These contributed to the elegant design of all-fiber optical system with high efficiency, high resolution and sensitivity of micro-photodetector, and enhanced interaction between the light and the samples at the liquid-sensor interface because of the large surface area of the multi-mode fiber probe. The LF-AOB can be extended as a universal sensing platform to measure other factors associated with refractive index because its high sensitivity, low sample consumption (~160 nL), and capability of real-time *in situ* detection.

* Corresponding author.
E-mail address: longf04@ruc.edu.cn (F. Long).
[1] These authors have equal contribution for this work.

https://doi.org/10.1016/j.aca.2021.338910
0003-2670/

1. Introduction

Optical biosensors have widely been applied for the clinical diagnostics, environmental monitoring, and food detection because of their significant advantages including smaller size, high sensitivity, strong anti-interference ability, easy-to-use, and easier integration [1–3]. Among them, label-free optical biosensors have attracted greater interests because the biomolecules can be detected close to their natural morphology without being changed by fluorescence or other markers in the binding process [4,5]. This is especially useful for protein targets due to the labels may compromise their function. Except for simplifying the detection operation, label-free methods benefit for the real-time interaction kinetic measurement of biomolecules [6]. To date, label-free optical biosensor based on refractive index (RI) is the most widely studied, applied, and successful method [7–11]. For example, surface plasmon resonance (SPR) biosensors are typically RI-response label-free and commercially available instruments (e.g. Biacore T200) and have become the golden standard in the real-time kinetic measurement of biomolecular interaction [8]. However, they require expensive and bulky instrument, time-consuming operation, and trained professional. SPR biosensors generally require to function a precious metal thin film on biosensing surface to produce surface plasmon resonance field. These make them be difficult to satisfy the increasing requirement of sensitive, cost-effective, and ease-of-use features in various applications [2,3].

In contrast, highly effective RI sensors can be designed using the Fresnel reflection principle [9–11]. In these systems, the reflectivity of the liquid-sensor interface is approximated by combining Fresnel reflection equations with Snell's law. Fresnel reflection-based fiber sensors embrace the ability of real-time *in situ* sensing and have a high tolerance for harsh environments. Several Fresnel reflection-based fiber RI sensors have been developed to measure RI, temperature, and other RI-associated factors [10–14]. Wu et al. developed a quasi-distributed Fresnel reflection-based fiber optic sensor to detect solute concentrations [12]. A Fresnel reflection-based fiber sensor was applied for multipoint RI measurements using arrayed waveguide grating [15]. Fresnel reflection-based fiber RI sensors had also been used for *in situ* polymerization monitoring via RI measurement [16,17]. However, to our best knowledge, no Fresnel reflection-based fiber sensors have been applied for detecting biomolecules (e.g. protein). Several factors are responsive for this. First, the end-surface of their transducers produced by single-mode fiber (SMF) is so small that the light-coupling efficiency and light-matter interaction is very low [4], thus resulting in a low detection of limit (LOD). Second, to eliminate the influence of light source power fluctuations, the aforementioned systems employed two fiber probes, a complex fiber coupler structure, and two photodetectors to detect the Fresnel reflection light signals of the sample and reference channels, respectively [14,16]. The relative Fresnel reflection ratio of both channels was used to determine liquid RI. The design of double channels rendered the entire system to be complex, costly, and impractical, especially for biomolecule detection. In addition, SMF-based RI sensors were easily bent in response to externally applied forces. Deformed SMF-based RI sensors reduced light transmission efficiency and generated inaccurate detection results [9,18].

To address these questions, a simple, compact label-free all-fiber optofluidic biosensor (LF-AOB) based on Fresnel reflection was designed for real-time *in situ* measurement of biomolecules. Unlike traditional fiber-based RI sensors, LF-AOB employs a single-multimode fiber coupler (SMFC) to transmit incident light and collect and transmit Fresnel reflected light. Because the entire system comprises non-bulk optical elements and requires no rigorous optical alignment, the elegant configuration design simplifies the overall optical structure and improves light transmission efficiency and stability. A commercially available multimode fiber substituting for SMF serves as a transducer and a biorecognition element after it is modified by biomolecules. As it has a relatively larger surface, the multimode fiber based biosensor enhances the interaction between the light and the targets in the sensing interface and improves LF-AOB sensitivity. A 635-nm laser is introduced into the multimode fiber probe through the SMFC. The incident light is reflected from the liquid-transducer interface and detected by a highly sensitive micro-photodetector produced by our group. Based on our theory, the RI change on the sensing interface can be detected *in situ* at high resolution and sensitivity by calculating the relative Fresnel reflection ratio without the reference channel. The feasibility of the proposed method was verified by *in situ* measurement of NaCl and protein solutions. In line with this, the LF-AOB was also applied for the real-time measurement of biomolecules interaction and sensitive detection of target biomolecules.

2. Experimental section

2.1. Materials and chemicals

SARS-Cov-2 Spike protein receptor-binding domain (S-RBD) and anti-S-RBD antibody were purchased from Beijing Biodragon Immunotechnologies CO., Ltd. (Beijing, China). Normal human IgG antibody were purchased from Wuhan Fine Biotech Co. Ltd. (Wuhan, China). The phosphate buffered saline solution (PBS, 137 mmol/L NaCl, 2.7 mmol/L KCl, 4.3 mmol/L Na_2HPO_4, and 1.4 mmol/L KH_2PO_4, pH = 7.4) and the antibody dilution buffer (1.0 g BSA, 0.02 g NaN_3 and 100 mL PBS) were prepared, respectively. The antibody stock solution was prepared by the antibody dilution buffer. Bovine serum albumin (BSA), 3-Mercaptopropyltrimethoxysilane (MTS), N-(4-maleimidobutyryloxy) succinimide (GMBS) were purchased from Sigma-Aldrich (Steinheim, Germany). The sodium dodecyl sulfate (SDS, 0.5%, pH = 1.9) was used to regenerate the bio-probe. All other reagents, unless specified, were supplied by Beijing Chemical Agents (Beijing, China). NaCl solutions of various concentrations were prepared by deionized water.

2.2. LF-AOB design and its sensing mechanism

The LF-AOB configuration is shown in Fig. 1, which consists of a multimode fiber probe, SMFC, a laser light source, a micro-photodetector (SOP-1000), and an optofluidic cell (Fig. 1). A 1-mW laser diode (LD; 635 nm) with a pigtail was selected as the light source as it is monochrome, inexpensive, and miniaturized. A commercial multimode fiber (NA = 0.22; length = 5.0 cm) was employed as a transducer and a biorecognition element after modified by biomolecules. The SMFC, consisting of a single mode fiber (4 μm, NA = 0.14) and a multi-mode fiber (600 μm, NA = 0.22), was used for the transmission of incident light and Fresnel reflection light. Using the SMFC, the incident light was introduced into the fiber probe embedded in the optofluidic cell. The optofluidic cell with an input port and an output port was made of the polyoxymethylene material using 3D printing. The dimensions of the cell with were ϕ600 μm × 600 μm and its effective volume was about 160 nL. Various liquids were peristaltically pumped into the optofluidic cell at 1.0 μL/min. The incident light transmitted within

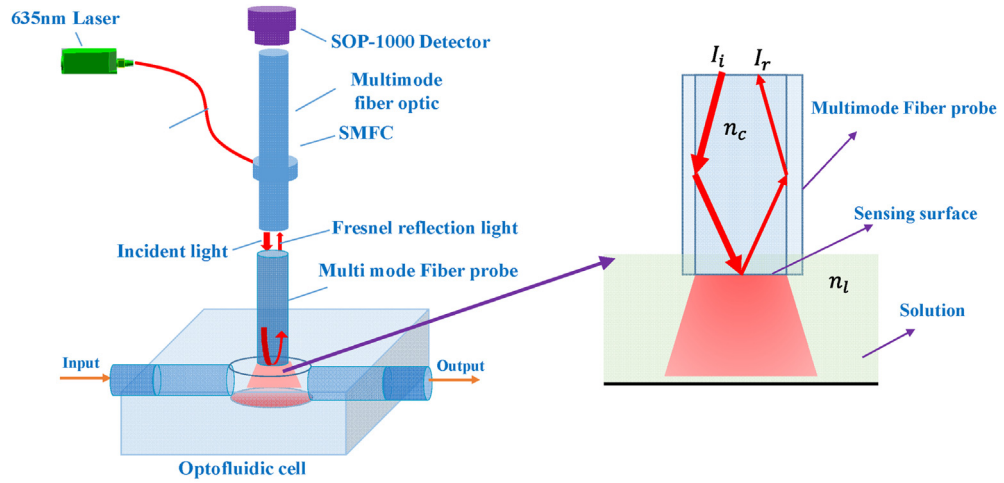

Fig. 1. LF-AOB design based on Fresnel reflection. (a) LF-AOB consisted of a multimode fiber probe, SFMC, laser, micro-photodetector (SOP-1000), and optofluidic cell. (b) Fiber probe immersed in liquid and its sensing principle. The incident light is introduced the sensing surface using SFMC, a fraction of the incident light is reflected and collected by the multimode SMFC fiber, which is detected in real time by the SOP-1000 detector.

the fiber probe core. According to the Snell-Descartes laws, a fraction of the incident light was reflected on the end surface of the fiber probe, collected by the multimode SMFC fiber, and detected in real time by the SOP-1000 detector.

In the LF-AOB system, the multimode fiber probe is used for bio/chemical analysis, whose diameter (Φ 600 μm) far surpasses the light wavelength. Therefore, a geometric optics model is applied for theoretical analysis and the LF-AOB RI response can be clarified. The reflection coefficients r_s and r_p for s- and p-polarizations at the liquid-sensor interface are calculated by Eqs. (1) and (2), respectively:

$$r_s = \frac{n_c \cos\theta - n_l \sqrt{1 - \left(\frac{n_c}{n_l}\sin\theta\right)^2}}{n_c \cos\theta + n_l \sqrt{1 - \left(\frac{n_c}{n_l}\sin\theta\right)^2}} \tag{1}$$

$$r_p = \frac{n_l \cos\theta - n_c \sqrt{1 - \left(\frac{n_c}{n_l}\sin\theta\right)^2}}{n_l \cos\theta + n_c \sqrt{1 - \left(\frac{n_c}{n_l}\sin\theta\right)^2}} \tag{2}$$

where n_c and n_l are the RI of the fiber core and tested solution, respectively, and θ is the angle of the incident laser light. The total reflectivity is calculated by Eq. (3):

$$\overline{R} = \frac{|r_s|^2 + |r_p|^2}{2} \tag{3}$$

The incidence light arrives at the end surface of fiber probe, and part of them is reflected based on Fresnel reflection principle and arrives at another end of the multimode fiber probe. The reflection light is collected by the multimode fiber of the SMFC and detected by the photodetector. The reflection light intensity between the incident angles θ and $\theta + d\theta$ could be written as.

$$dI \propto I(\theta) d(\theta) \tag{4}$$

where the mode intensity corresponding to the incident angle θ is

$$I(\theta) = \frac{n_c^2 \sin\theta \cos\theta}{\left(1 - n_c^2 \cos^2\theta\right)^2} \tag{5}$$

When the fiber probe is immersed in the target liquid, the Fresnel reflection intensity will be derived as Eq. (6), by using the reflection value for a single reflection at fiber probe interface.

$$I_l = \int_0^{\theta} \overline{R}\% I(\theta)\, d\theta \tag{6}$$

To eliminate system errors originating from light source instability, fiber connector coupling loss, or fiber probe differences, the reference light intensity was adopted when the multimode fiber probe was immersed in ultrapure water with known RI n_w. I_w collected by SOP-1000 was determined as follows:

$$I_w = \int_0^{\theta} \overline{R_w}\% I(\theta)\, d\theta \tag{7}$$

From Eqs. (6) and (7), the relative Fresnel reflected light intensity ratio R was calculated as follows.

$$R = \frac{I_l}{I_w} = \frac{\int_0^{\theta} \overline{R}\% I(\theta)\, d\theta}{\int_0^{\theta} \overline{R_w}\% I(\theta)\, d\theta} \tag{8}$$

The SMF NA of the SMFC was 0.14. Hence, the incidence light transmission angle (θ) was <8.1° when it transmitted in the fiber probe via total internal reflection. Therefore, Eq. (8) can be simplified as,

$$R = \frac{I_l}{I_w} = K\% \left(\frac{n_c - n_l}{n_c + n_l}\right)^2 \quad (9)$$

where K is a constant. From this, the R is only relative to the RI of the fiber probe surface. Eq. (9) can be rewritten as,

$$n_l = n_c \left(\frac{1-\alpha}{1+\alpha}\right) \quad (10)$$

where $\alpha = \left(\frac{R}{K}\right)^{1/2}$. Therefore, the RI change of fiber probe surface can be determined through detecting the ratio of reflection light intensity of target solution and pure water.

The RI of a liquid is a function of its concentration C, the temperature T, and the incident light wavelength [19]. However, the effects of temperature and incident light wavelength on the change in liquid RI could be ignored here as the light source (635 nm LD) was highly monochromatic and the temperature variation was controlled within 1–2 °C throughout the experiment. For most liquids, the order of magnitude of the temperature is ~1×10^{-4} °C. Therefore, the relationship between liquid concentration (C) and RI may be expressed as following [20]:

$$n_l = \left(\frac{\partial n}{\partial C}\right)\%C + n_0 \quad (11)$$

where n_0 is the RI of blank solution.

Because the Fresnel reflection light intensity greatly depends on the RI change of the fiber probe interface, the change of liquid concentration in the optofluidic cell or biomolecules binding reaction alters the RI of the sensing interface, thus changing the Fresnel reflected light intensity. By combining eqs. (8), (10) and (11), the liquid RI or target concentration can be determined according to the relative Fresnel reflected light intensity ratio.

2.3. Preparation of fiber bio-probe by immobilizing biorecognition molecules

For SARS-Cov-2 S-RBD biosensing, anti-S-RBD antibody was modified onto the end surface of multimode fiber probe as previously reported with minor modifications [21]. The fiber probe was immersed in piranha solution (H_2SO_4: H_2O_2 = 3:1) for 30 min. The fiber probe was rinsed, dried, and immersed in 2% APTES in toluene for 2 h to coat it with a reactive silane layer. It was then rinsed with ultrapure water, dried in a nitrogen gas stream, and immersed in a heterobifunctional crosslinker solution (4% glutaraldehyde) for 1 h to react with the amino groups in the silane coating. The fiber probe was then functionalized with 1.0 mg/mL anti-S-RBD antibody for 2 h, rinsed with PBS, immersed in 2.0 mg/mL BSA to block nonspecific adsorption sites, and stored at 4 °C until use.

2.4. Detection of NaCl and BSA solutions using the LF-AOB

To evaluate the LF-AOB sensing performance, a multimode fiber probe was placed in the optofluidic cell. NaCl solutions (0–20%, w/v) and BSA solutions (0–30 mg/mL) of various concentrations were sequentially introduced into the cell and the Fresnel reflected light intensities were real time detected by the LF-AOB, respectively.

2.5. Detection of SARS-CoV-2 S-RBD using the LF-AOB

To achieve biosensing of SARS-CoV-2 S-RBD, anti-S-RBD antibody modified fiber bio-probe was embedded in the optofluidic cell. Different concentrations of SARS-CoV-2 S-RBD were introduced into the cell, and the Fresnel reflected light intensity was detected using the LF-AOB for 400s reaction.

3. Results and discussion

3.1. LF-AOB characteristics

In the LF-AOB system, the incident light is introduced into the fiber probe through the SMFC and the Fresnel reflected light from the probe end surface is detected by the SOP-1000. Stable LD light intensity is essential for LF-AOB performance. Here, a single 635-nm LD with a pigtail served as the light source because it was monochrome, inexpensive, and miniaturized. Stability of the LD light intensity was established by detecting the Fresnel reflected light intensity when the fiber probe was immersed in water (Fig. 2a). The Fresnel reflected light intensity detected by the SOP-1000 remained constant after the LD was powered on and its variance was within ±0.01%. Hence, the LD was sufficiently stable for RI detection.

To assess the feasibility of our design, we evaluated the response of the LF-AOB system to RI variation. Fig. 2a shows typical light intensity signal traces when water and various NaCl solutions are introduced over the fiber probe, respectively. The Fresnel reflected light intensity was virtually unchanged when water was pumped into the optofluidic cell. When 10% (w/v) NaCl flowed over the fiber probe, the reflected light intensity sharply decreased as relatively less light was reflected (Eq. (6)). Even greater reflected light intensity attenuation was observed when 20% (w/v) NaCl was introduced into the optofluidic cell because this solution had a comparatively higher RI. These results confirmed that LF-AOB was sensitive to RI variations. When the fiber probe was fully immersed into the NaCl solution, the detectable light intensity remained constant, which further demonstrated the stability of the LF-AOB. To evaluate the Fresnel reflection efficiency of the fiber probe end face, we used the finite-difference time-domain (FDTD) to simulate the electronic field intensity when the probe was immersed in various RI solutions. Fig. 2b–d shows that the electronic field intensity decreased with increasing solution RI. This finding was consistent with the experimental results. After the probe was rinsed with water, the light intensity increased and was restored to its original value. Fig. 2a shows that the fall and rise times are very short (<15 s). Thus, LF-AOB rapidly responded to the RI variations.

The attenuation light intensity value (ΔI) was obtained by subtracting the light intensity value at each concentration from the baseline light intensity value as follows:

$$\Delta I = \text{reflection light intensity at baseline} - \text{reflection light intensity at each concentration} \quad (12)$$

3.2. Sensing performance evaluation of the LF-AOB

To evaluate the LF-AOB sensing performance, NaCl solutions of various concentrations were sequentially introduced into the cell and the Fresnel reflected light intensities were real time detected. Typical signal traces are shown in Fig. 3a. The reflected light intensities decreased with increasing NaCl concentration, which resulted to the increase of the RI at the liquid-sensor interface. As the NaCl concentration increased from 0 to 20% (w/v), the reflection light intensity decreased from 36,200 to 24,030. The reflection light intensity attenuation values and NaCl concentrations were plotted and an excellent linear relationship was obtained ($y = 594.57x + 7.22$, $R^2 = 0.9988$) (Fig. 3b). The error bars in Fig. 3b corresponded to the standard deviation (SD) for triplicate

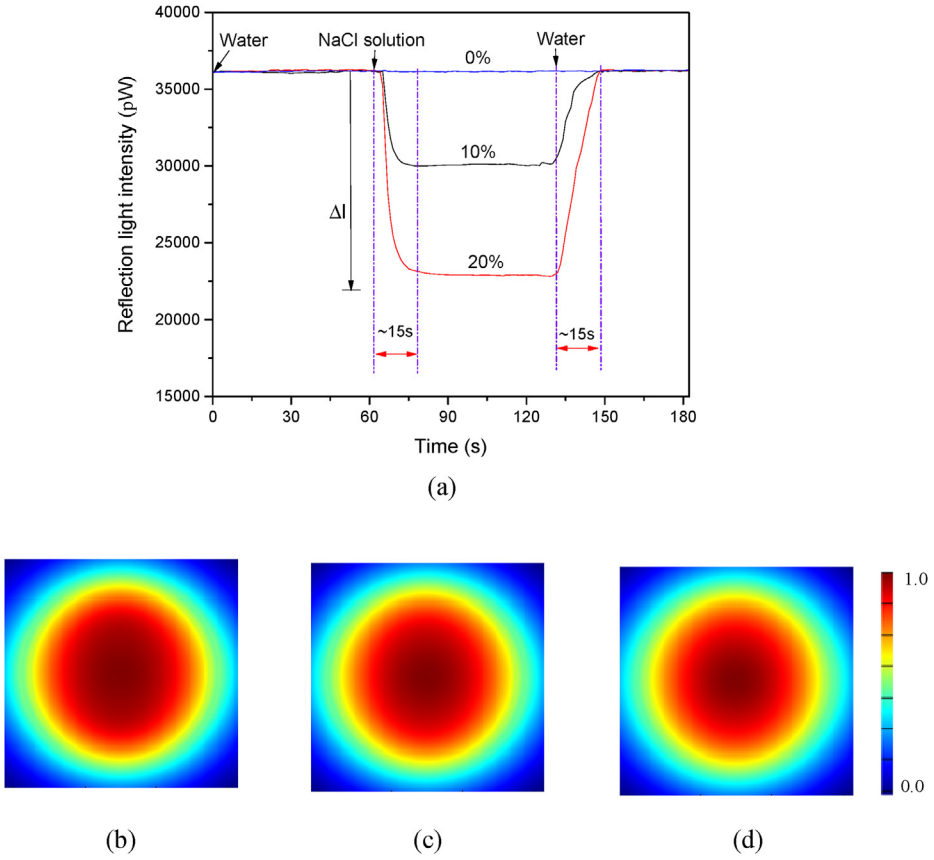

Fig. 2. LF-AOB characteristics. (a) Real-time Fresnel reflected light intensities for various NaCl solutions (0%, 10%, and 20% (w/v)) introduced into optofluidic cell. (b) (c) and (d) show electronic field intensity profiles in fiber probe end face when it immersed in 0%, 10%, and 20% (w/v) NaCl, respectively.

experiments, and all of them were <1.5%, indicating the good stability of the LF-AOB. Fig. 3b shows that the limit of detection (LOD) for NaCl solution using 3 × SD of the mean blank values was 0.12%. The signal trace always returned to baseline after the NaCl solution was rinsed off with water. Both the fall and rise times were ~15 s, indicating the rapid response of the LF-AOB on the RI change.

Fig. 3c shows the measured Fresnel light intensity as a function of the NaCl solution RI. The sensor sensitivity was defined as $\triangle I/\triangle n$, where $\triangle I$ was the change in Fresnel light intensity and $\triangle n$ was the change in solution RI on the liquid-sensor surface. Fig. 3c shows that the sensitivity is 5.02×10^5 pW/RIU (RI unit). The LOD is an important RI sensor parameter. It was defined as the ratio of the smallest decrease in reflected light intensity measurable in the presence of noise to the RI sensor sensitivity [20]. The LF-AOB mini-photodetector resolution was 0.5 pW at 635 nm. Hence, the LOD for LF-AOB was 1.0×10^{-6} RIU. This enhanced sensor sensitivity could be attributed to the elegant design of the all-fiber optical system in the LF-AOB. The SMFC augments light transmission efficiency and diminishes light loss. Moreover, multimode fiber probes furnished large specific surface areas that accentuated the interactions between the incident light and the samples in the optofluidic system. In this way, they increased overall sensitivity to RI changes. Finally, our photodetectors with good resolution further improved the sensitivity of the entire system.

The NaCl concentrations were determined from the linear relationship between them and the reflected light intensity attenuation value (Fig. 3b). However, the use of different fiber probes and fiber connector couplings might alter the incident light intensity (I_0) and, by extension, the reflected light intensity attenuation value [12,14]. Therefore, a new calibration curve must be plotted each time in order to obtain accurate detection results. The liquid RI could be calculated from Eq. (10) as it only depended on the R value. Equation (9) shows that R is independent of the incidence intensity (I_0). Thus, the reflected light intensity of ultrapure water might serve as a reference value to eliminate the influences of incident light intensity fluctuations. This manipulation was validated by assessing the influences of light intensity fluctuations simulated by altering the incident light power. Fig. S1 shows the relative deviation changes with light intensity attenuation. The RI variation was <0.5% when the light intensity fluctuation exceeded 20%. Thus, the impact of incident light intensity fluctuation might be eliminated by the relative light intensity method.

Fig. 3d displays a calibration curve for the NaCl concentrations and their corresponding RIs calculated with Eq. (10). There was a good linear relationship within the experimental NaCl concentration range and the LOD was 0.12%. The calculated RIs for various NaCl concentrations were slightly lower than those detected with an Abbe refractor possibly because the latter used different light sources (Table S1) [20]. Nevertheless, there was a good linear relationship between these factors (Fig. S2). Therefore, the NaCl concentrations might be determined from the changes in relative Fresnel light intensity when ultrapure water was the reference liquid introduced into the cell to obtain the reference signal I_0. After the reflected light intensities of the NaCl solutions were measured, the NaCl concentration could be rapidly determined based on the relative light intensity using the one-point calibration method. This approach facilitated practical LF-AOB application.

Table S2 compares the characteristics of the LF-AOB with those

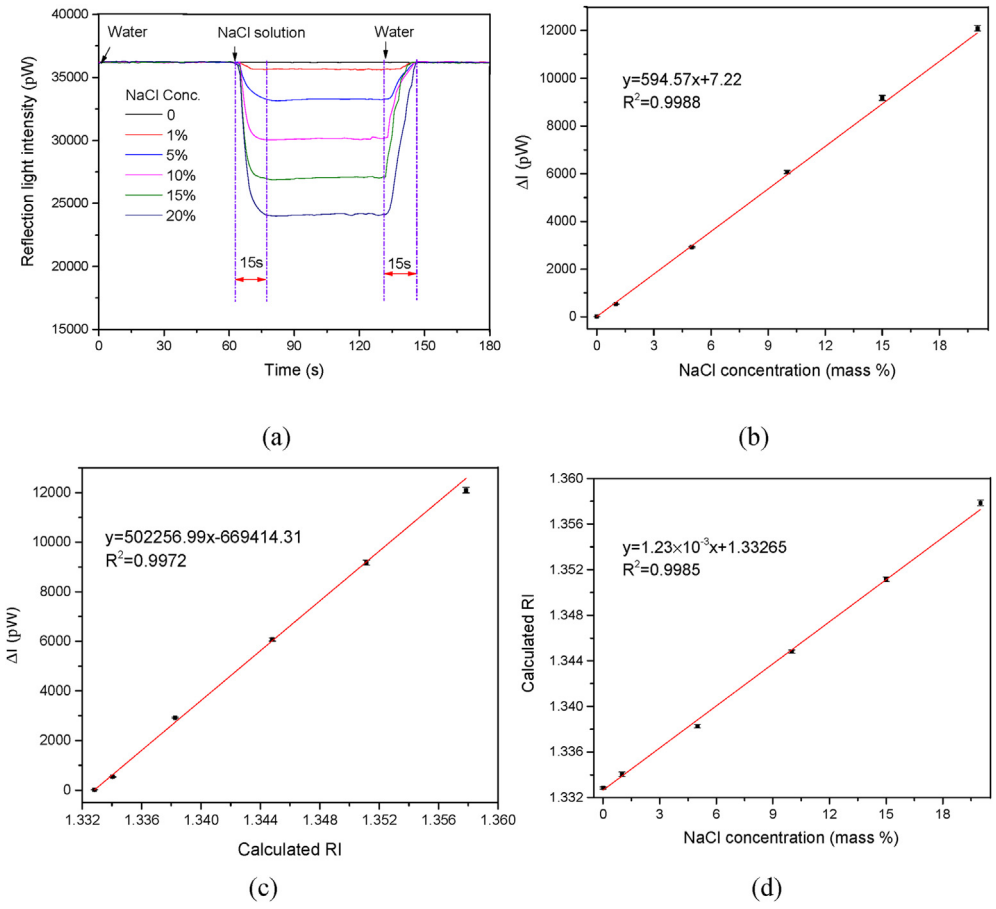

Fig. 3. Sensing performance evaluation of the LF-AOB using NaCl solution. (a) Typical signal curves for various NaCl concentrations. (b) Plot of reflected light intensity attenuation value as a function of change in NaCl concentration. (c) Plot of reflected light intensity attenuation value as a function of change in calculated RI. (d) Plot of calculated RI as a function of change in NaCl concentration. Fitted linear equations and R^2 are shown. Error bars correspond to SD for triplicate experiments (n = 3).

of other optical RI sensors. The LOD of the LF-AOB was lower than those of other sensors. It should be noted that only one fiber coupler and one fiber probe were required for the LF-AOB system. Hence, its structure was simple and benefited to perform *in situ* RI detection on very small liquid sample volumes (~160 nL) in optofluidic systems. Instead of using the reflection light of the other air-sensor surface as reference signal [14,20], the proposed one-point calibration method can not only eliminate the influence of incidence light intensity fluctuation, but also self-calibrate sensor performance without redundant optical components. This is essential for practical applications of the optical RI sensors.

3.3. Detection of protein in solution

The protein concentration is an important factor in bioassays and clinical diagnoses [22]. To validate the potential of the LF-AOB as a biosensor, we measured BSA concentrations in PBS. Fig. 4a shows typical signal traces when various BSA concentrations are sequentially introduced into the optofluidic cell. The Fresnel reflected light intensity decreased with increasing BSA concentration. There was a good linear relationship between the reflected light intensity attenuation value and the BSA concentration (Fig. S3). The signal trace always returned to the baseline after the BSA solution was rinsed off with water and the rise time was ~20 s. The BSA fall and rise times were longer than those for the NaCl solutions, corresponding to that the BSA solution viscosities were higher than those of the NaCl solutions. The absorption of BSA on the probe surface might be another reason.

To minimize the influences of incident light fluctuation, we plotted the relationship between the calculated RI and the protein concentration (Fig. S4), and a good linear relationship was obtained. Fig. S4 shows that the protein RI increments ($\partial n_p/\partial C_p$) can be determined. These values played vital roles in the detection of target proteins such as cancer biomarkers by analytical ultracentrifugation (AUC) and with various label-free optical biosensors [23,24]. Numerous technologies have been developed to measure protein RI increments [23,25]. The BSA RI increments ($\partial n_p/\partial C_p$) determined here was 1.705×10^{-4} mL/mg and closely approached a previously reported value (1.71×10^{-4} mL/mg) of BSA in previous reports [23,25]. Hence, our proposed method was feasible and the linear fitting was accurate. Compared with other methods, the LF-AOB was simpler and more cost-effective. In this study, the BSA RI increased from 1.3342 to 1.3393 when its concentration increased from 0 to 30 mg/mL. Fig. 4b shows a good linear relationship between the calculated RIs and the BSA concentration. The calculated RI of BSA solution were almost consistent with those detected by an Abbe refractor (Table S3). Thus, the LF-AOB and one-point calibration methods could be practically applied to determine BSA concentrations. The sensitivity of the LF-AOB for BSA detection in PBS was 3.07×10^5 pW/RIU and the LOD was ~1.6×10^{-6} RIU.

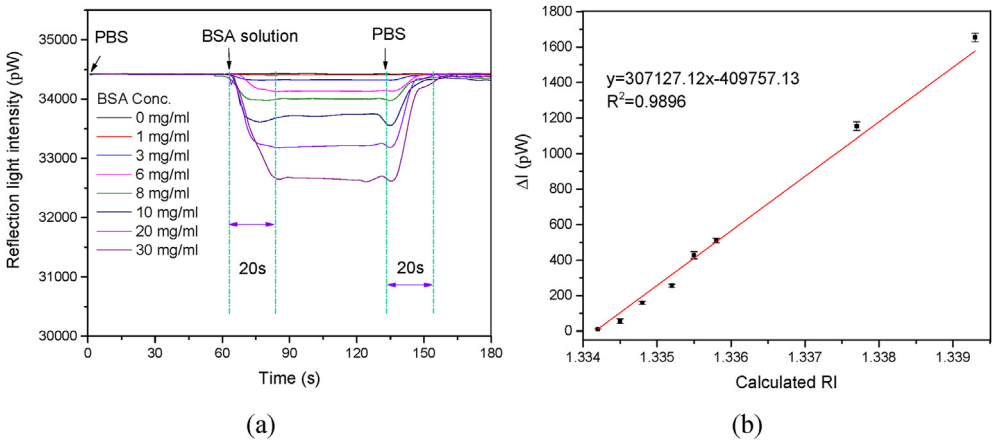

Fig. 4. Protein detection using the LF-AOB. (a) Typical signal curves for various BSA concentrations. (b) Plot of reflected light intensity attenuation value as a function of change in calculated RI. Fitted linear fitted equations and R^2 are shown.

3.4. Characteristics of anti-S-RBD antibody functionalized fiber bio-probe

The anti-S-RBD antibody functionalized fiber bio-probe was vertically immersed into the optofluidic cell, and several control experiments were performed (Fig. 3A). First, various control samples, such as PBS, BSA, OVA, and normal human IgG, were introduced into the optofluidic cell. The Fresnel reflection light intensity rarely decreased even when the control protein (e.g. BSA, OVA, or normal human IgG) concentration was as high as 1000 ng/mL. However, the Fresnel reflection light intensity decreased over the time when the 1 ng/mL SARS-CoV-2 S-RBD protein solution was introduced over the bio-probe surface. Although its concentration was 1000 times lower than those of other control proteins, the decrease value of Fresnel reflection light intensity was higher than those originated from other control proteins (Fig. 5). This contributed to that the SARS-CoV-2 S-RBD specifically bound with the anti- S-RBD antibody functionalized fiber bio-probe surface, which raised the local RI of the biosensing surface and allowed the less lights to reflect according to Eq. (9). When the higher concentration of SARS-CoV-2 S-RBD protein solution (10 ng/mL) was added, the bigger decrease of Fresnel reflection light intensity was observed. These results showed that the anti-S-RBD antibody was successfully modified onto the bio-probe, and the observed Fresnel reflection light intensity decrease originated from the target protein specifically bound with the captured antibody. Based on Fresnel reflection principle, the LF-AOB could be applied for the label-free detection of SARS-CoV-2 S-RBD protein.

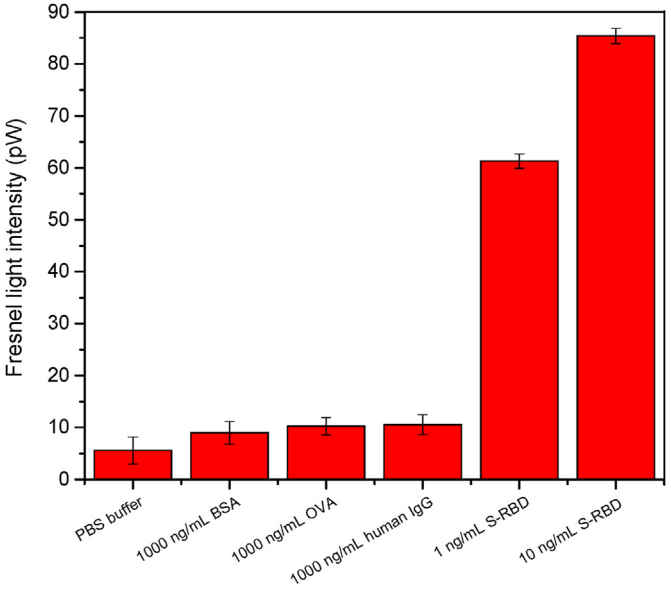

Fig. 5. Response of the anti-S-RBD antibody functionalized bio-probe for PBS, BSA, OVA, normal human IgG, and SARS-CoV-2 S-RBD, respectively. Reaction time were 400 s. Error bars corresponded to the standard deviation (SD) of data points in triple experiments.

3.5. Detection of SARS-CoV-2 S-RBD using the LF-AOB

The COVID-19 pandemic triggered by severe acute respiratory syndrome coronavirus 2 (SARS-CoV-2) has become the biggest public-health crisis in a century. SARS-CoV-2 used its S-RBD to bind with the host cell receptor angiotensin-converting enzyme 2(ACE2), which was the most essential step during infection [26,27]. Developing the antibodies that specifically recognized the virus with high affinity was one major method to debate this pandemic, because they bound to the viral spike protein and hindered spike-protein function, thus blocking infection [28]. Therefore, understanding the interactions between spike protein and antibodies is essential for the antibody product, clinical diagnosis, and vaccine [28].

Before this, a simple biomolecular interaction model for immunoassay was built provided the following assumptions. (a) the biosensing surface is a homogenous monolayer; (b) the immunoassay between protein and its antibody follows first-order kinetics; (c) no interactions between binding sites exist; (d) the number of targets in solution is far higher than that of the bio-recognition molecule sites on the biosensing surface, and (e) the mass transport flux is much faster than the reaction rate [29]. The binding dynamics between antigen (Ag) and antibody (Ab) can be expressed as follows [30].

$$P + A \rightleftarrows \frac{k_{on}}{K_{off}} P\%A \tag{13}$$

where k_{on} and k_{off} are the forward and reverse rate constants for the formation and dissociation of an affinity complex (P•A), respectively. The binding kinetic equation between the antigen and antibody on the biosensing surface can be written as following.

$$\frac{\partial[P \bullet A]}{\partial t} = k_{on}[P]_0[A]_0 - \left(k_{on}[A]_0 + k_{off}\right)[P \bullet A] \quad (14)$$

where [P•A] is the time-dependent concentration of the SARS-CoV-2 S-RBD/anti-S-RBD antibody complex, $[A]_0$ is the initial concentration of S-RBD, and $[P]_0$ is the S-RBD antibody on the biosensing surface. According to eq. (14), the equilibrium association constant of K_a (k_{on}/k_{off}) between S-RBD/anti-S-RBD antibody could be obtained by using real-time kinetic curves S-RBD bound with antibodies.

To evaluate the performance of LF-AOB as a label-free device for biomolecular interaction analysis, various concentrations of SARS-CoV-2 S-RBD was introduced over the fiber bio-probe modified by anti-S-RBD antibody. Typical signal traces are shown in Fig. 6a. The reflected light intensity decreased with time after the SARS-CoV-2 S-RBD was added as it specifically bound the anti-S-RBD antibody, which resulted in the RI increase of the fiber bio-probe end face and reduced Fresnel reflected light intensity. As expected, the reflected light intensity attenuation values increased with increasing SARS-CoV-2 S-RBD concentration. The dose-response curve of S-RBD were demonstrated in Fig. 6b, which were plotted against the logarithm of the concentration of S-RBD using a four-parameter logistic equation (Supporting information). The affinity constant K_a between SARS-CoV-2 S-RBD and anti-S-RBD antibody was determined as and 2.96×10^{10} M^{-1}. The LOD for SARS-CoV-2 S-RBD was 0.005 ng/mL according to three SD of the mean blank values. Although we did not detect the SARS-CoV-2 virus because of the limit of experimental conditions, the LF-AOB could obviously be applied for the direct detection of SARS-CoV-2 virus using anti-S-RBD antibody functionalized fiber bio-probe. These results demonstrated that the LF-AOB could serve as a simple, label-free biosensing platform for biomolecular quantitation and binding kinetics assay between biomolecules. Compared with traditional label-free biosensors [8,30], the LF-AOB have several advantages as followings. First, the precious metal thin film on biosensing surface required in the SPR biosensors is unnecessary, which is complicate, expensive, and time-consuming. Second, the SiO_2 surface of multi-mode fiber probe benefits for the modification of more bio-recognition molecules, thus improving the sensitivity of the system. In addition, the LF-AOB is simpler, compact, and easy-to-use.

4. Conclusion

A simple, compact, cost-effective, and robust all-fiber optofluidic biosensor based on Fresnel reflection principle was designed and constructed through integrating an all-fiber optical system and a highly sensitive micro-photodetector. Our results demonstrated that the LF-AOB conceived in this work could perform real time *in situ* detection of various liquids (e.g. NaCl and BSA solutions) in optofluidic systems. The LF-AOB had the highest sensitivity of 5.02×10^5 pW/RIU and the lowest LOD of 1.0×10^{-6} RIU, which contributed to the elegant design of all-fiber optical system with high efficiency, high-resolution photodetector, and the enhanced interaction of the light and the sample at the liquid-sensor interface because of the large surface area of the multimode fiber probe. The experimental results corroborated our theory demonstrated that the influences of light intensity fluctuation could be eliminated and one-point sensor self-calibration was feasible, which benefited for its practical applications. The LF-AOB may also serve as a label-free biosensor for sensitive detection of biomolecules with several outstanding features, such as free precious metal thin film required in the SPR biosensors, easy-to-modification biosensing surface, and simpler and compact system structure. Moreover, the LF-AOB may also be extended as a universal biosensing platform to measure other factors associated with the refractive index because its high sensitivity, low sample consumption (~160 nL), and capability of real-time *in situ* detection.

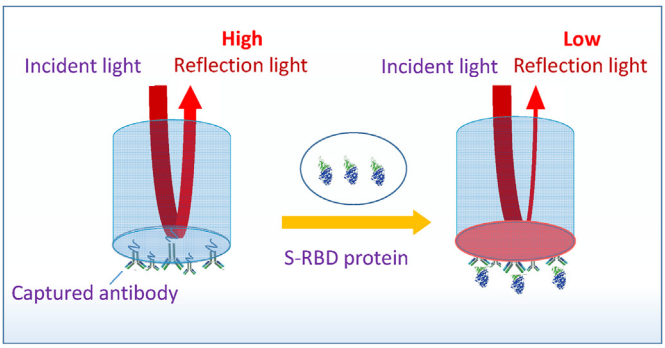

(a)

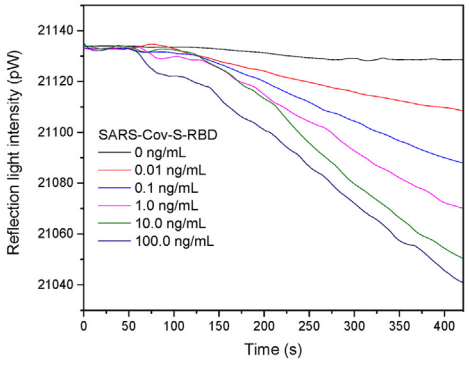

(b)

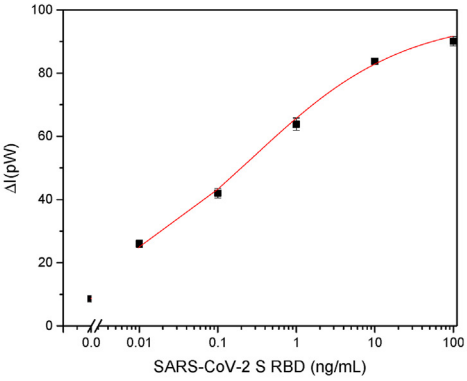

(c)

Fig. 6. Detection of SARS-Cov-2 S-RBD using the LF-AOB. (a) Schematic of immunosensing mechanism of SARS-CoV-2 S-RBD using the LF-AOB based on Fresnel reflection and immunoassay. The SARS-CoV-2 S-RBD protein binds with the captured antibody anti-S-RBD antibody immobilized on the fiber bio-probe, which reduces the reflection light intensity. (b) Typical signal curves of S-RBD detection using the LF-AOB; (c) Dose-response curve of S-RBD detection based on bifunctional bio-probe. The error bars corresponded to the standard deviation of the data points in three repeated experiments (n = 3).

CRediT authorship contribution statement

Wenjuan Xu: performing all the experiments and writing the manuscript. **Yuxin Zhuo:** performing all the experiments and writing the manuscript. **Dan Song:** performing all the experiments and writing the manuscript. **Xiangzhi Han:** drawing and summarizing figures. **Jiaxin Xu:** drawing and summarizing figures. **Feng Long:** drawing and summarizing figures, designing, managing the project, and Editing, All the authors discuss the results and commented on the manuscript.

Declaration of competing interest

The authors declare that they have no known competing financial interests or personal relationships that could have appeared to influence the work reported in this paper.

Acknowledgements

This work was supported by the National Natural Science Foundation of China (21675171); and the National Key Scientific Instrument and Equipment Development Projects of China (2012YQ3011105).

Appendix A. Supplementary data

Supplementary data to this article can be found online at https://doi.org/10.1016/j.aca.2021.338910.

References

[1] J.J.S. Rickard, V. Di-Pietro, D.J. Smith, D.J. Davies, A. Belli, P.G. Oppenheimer, Rapid optofluidic detection of biomarkers for traumatic brain injury via surface-enhanced Raman spectroscopy, Nat. Biomed. Eng 4 (2020) 610–623.
[2] X. Fan, I.M. White, Optofluidic microsystems for chemical and biological analysis, Nat. Photonics 5 (2011) 591–597.
[3] D. Psaltis, S.R. Quake, C. Yang, Developing optofluidic technology through the fusion of microfluidics and optics, Nature 442 (2006) 381–386.
[4] Y. Wang, G. Zhao, H. Chi, S. Yang, Q. Niu, D. Wu, W. Cao, T. Li, H. Ma, Q. Wei, Self-luminescent lanthanide metal–organic frameworks as signal probes in electrochemiluminescence immunoassay, J. Am. Chem. Soc. 143 (2021) 504–512.
[5] S. Zeng, D. Baillargeat, H.P. Ho, K.T. Yong, Nanomaterials enhanced surface plasmon resonance for biological and chemical sensing applications, Chem. Soc. Rev. 43 (2014) 3426–3452.
[6] C. Chen, R. Yang, X. Zhang, W. Wei, Q. Guo, X. Zhang, L. Qin, Y. Ning, Y. Yu, Compact refractive index sensor based on an S-tapered fiber probe, Opt. Mater. Express 8 (2018) 919.
[7] A.K. Sharma, R. Jha, B.D. Gupta, Fiber-optic sensors based on surface plasmon resonance: a comprehensive review, IEEE Sensor. J. 7 (2007) 1118–1129.
[8] A.M. Holtz, S.C. Griffiths, S.J. Davis, B. Bishop, C. Siebold, B.L. Allen, Secreted HHIP1 interacts with heparan sulfate and regulates Hedgehog ligand localization and function, J. Cell Biol. 209 (2015) 739–758.
[9] Y. Luo, R. Fan, Y. Zhang, Q. Wu, Z. Ren, B. Peng, Novel optical fiber refractive sensor fabricated with an alcohol-filled photonic crystal fiber based on a Mach–Zehnder interferometer, Opt. Fiber Technol. 48 (2019) 278–282.
[10] B. Wang, K. Ni, P. Wang, Q. Ma, W. Tian, L. Tan, A CNT-coated refractive index sensor based on Michelson interferometer with thin-core fiber, Opt. Fiber Technol. 46 (2018) 302–305.
[11] L. Zhang, Z. Zhang, Y. Wang, M. Ye, W. Fang, L. Tong, Optofluidic refractive index sensor based on partial reflection, Photonic Sensors 7 (2017) 97–104.
[12] Y.T. Wu, X.G. Huang, H. Su, A quasidistributed fiber optic sensor for solute concentration measurement based on Fresnel reflection, Appl. Phys. Lett. 91 (2007) 131101.
[13] J.R. Zhao, X.G. Huang, J.H. Chen, A Fresnel-reflection-based fiber sensor for simultaneous measurement of liquid concentration and temperature, J. Appl. Phys. 106 (2009) 331.
[14] P.Q. Zhu, J.J. Wang, F. Rao, C. Yu, G. Zhou, X.G. Huang, Differential Fresnel-reflection-based fiber biochemical sensor with temperature self-compensation for high-resolution measurement of Cd2+ concentration in solution, Sensor. Actuator. B Chem. 282 (2019) 644–649.
[15] C.L. Zhao, J. Li, S. Zhang, Z. Zhang, S. Jin, Simple fresnel reflection-based optical fiber sensor for multipoint refractive index measurement using an awg, IEEE Photon. Technol. Lett. 25 (2013) 606–608.
[16] X. Zhao, Z. Zhang, K. Guo, J. He, G. Zhou, X. Huang, Fresnel-reflection-based fiber sensor for UV adhesive cure monitoring, Opt Commun. 474 (2020) 126099.
[17] R. Grangeat, M. Girard, C. Lupi, D. Leduc, F. Jacquemin, Measurement of the local water content of an epoxy adhesive by fiber optic sensor based on Fresnel reflection, Mech. Syst. Signal Process. 141 (2020) 106439.
[18] Y.C. Tan, W.B. Ji, V. Mamidala, K.K. Chow, S.C. Tjin, Carbon-nanotube-deposited long period fiber grating for continuous refractive index sensor applications, Sensor. Actuator. B Chem. 196 (2014) 260–264.
[19] V. Krishna, C.H. Fan, J.P. Longtin, Real-time precision concentration measurement for flowing liquid solutions, Rev. Sci. Instrum. 71 (2000) 3864–3868.
[20] H. Su, X.G. Huang, Fresnel-reflection-based fiber sensor for on-line measurement of solute concentration in solutions, Sensor. Actuator. B Chem. 126 (2007) 579–582.
[21] F. Long, M. He, A.N. Zhu, H.C. Shi, Portable optical immunosensor for highly sensitive detection of microcystin-LR in water samples, Biosens. Bioelectron. 24 (2009) 2346–2351.
[22] M. Pozuelo, P. Blondeau, M. Novell, F.J. Andrade, F. Xavier Rius, J. Riu, Paper-based chemiresistor for detection of ultralow concentrations of protein, Biosens. Bioelectron. 49 (2013) 462–465.
[23] H. Zhao, P.H. Brown, P. Schuck, On the distribution of protein refractive index increments, Biophys. J. 100 (2011) 2309–2317.
[24] F. Chiavaioli, P. Zubiate, I. Del Villar, C.R. Zamarrenìo, A. Giannetti, S. Tombelli, C. Trono, F.J. Arregui, I.R. Matias, F. Baldini, Femtomolar detection by nanocoated fiber label-free biosensors, ACS Sens. 3 (2018) 936–943.
[25] R. Barer, S. Tkaczyk, Refractive index of concentrated protein solutions [5], Nature 173 (1954) 821–822.
[26] C. Wang, P.W. Horby, F.G. Hayden, G.F. Gao, A novel coronavirus outbreak of global health concern, Lancet 395 (2020) 470–473.
[27] N. Zhu, D. Zhang, W. Wang, X. Li, B. Yang, J. Song, X. Zhao, B. Huang, W. Shi, R. Lu, P. Niu, F. Zhan, X. Ma, D. Wang, W. Xu, G. Wu, G.F. Gao, W. Tan, A novel coronavirus from patients with pneumonia in China, 2019, N. Engl. J. Med. 382 (2020) 727–733.
[28] R. Shi, C. Shan, X. Duan, Z. Chen, P. Liu, J. Song, T. Song, X. Bi, C. Han, L. Wu, G. Gao, X. Hu, Y. Zhang, Z. Tong, W. Huang, W.J. Liu, G. Wu, B. Zhang, L. Wang, J. Qi, H. Feng, F.S. Wang, Q. Wang, G.F. Gao, Z. Yuan, J. Yan, A human neutralizing antibody targets the receptor-binding site of SARS-CoV-2, Nature 548 (2020) 1–8.
[29] T.M. Squires, R.J. Messinger, S.R. Manalis, Making it stick: convection, reaction and diffusion in surface-based biosensors, Nat. Biotechnol. 26 (2008) 417–426.
[30] M. Fivash, E.M. Towler, R.J. Fisher, BIAcore for macromolecular interaction, Curr. Opin. Biotechnol. 9 (1998) 97–101.